

Showcasing research from the Laboratory of Molecular Structure and Dynamics, Institute of Chemistry, Eötvös University and the MTA-ELTE Research Group on Complex Chemical Systems, Budapest, Hungary.

Dynamics of the $F^- + CH_3Cl \rightarrow Cl^- + CH_3F$ S_N2 reaction on a chemically accurate potential energy surface

Reaction dynamics simulations on a new full-dimensional *ab initio* analytical potential energy surface reveal several mechanisms and outcomes for the $F^- + CH_3Cl$ prototypical S_N2 reaction.

As featured in:



See Gábor Czakó, *Chem. Sci.*, 2013, **4**, 4362.

RSC Publishing

www.rsc.org/chemicalscience

Registered Charity Number 207890

Dynamics of the $F^- + CH_3Cl \rightarrow Cl^- + CH_3F$ S_N2 reaction on a chemically accurate potential energy surface

Cite this: *Chem. Sci.*, 2013, **4**, 4362

István Szabó,^a Attila G. Császár^{ab} and Gábor Czako^{*a}

Though bimolecular nucleophilic substitution (S_N2) reactions play a fundamental role in chemistry, chemically accurate full-dimensional global analytical potential energy surfaces (PESs) have not been developed for these systems. These PESs govern the motion of the atoms in a chemical reaction; thus, the knowledge of the PES is essential to study the dynamics and atomic-level mechanisms. Here, we report a full-dimensional *ab initio* PES for the $F^- + CH_3Cl \rightarrow Cl^- + CH_3F$ reaction, the PES has an estimated average accuracy of about $0.5 \text{ kcal mol}^{-1}$. Quasiclassical trajectories on this PES reveal that the direct rebound mechanism dominates at high collision energies, whereas the reaction is mainly indirect at low collision energies, where the formation of long-lived hydrogen-bonded and C_{3v} ion-dipole entrance-channel complexes play a major role in the dynamics. A direct stripping mechanism is also found at large impact parameters resulting in significant forward scattering, whereas the direct rebound mechanism scatters towards backward directions. At high collision energies the reaction can be controlled by orienting the reactants into a reactive $F^- + H_3CCl$ orientation, whereas at low collision energies the initial orientation is not always maintained, because the long-range ion-dipole interactions efficiently steer the reactants into a reactive orientation even if F^- initially approaches the non-reactive side of CH_3Cl . Mode-specific vibrational distributions show that the reaction produces vibrationally hot CH_3F molecules with excited CF stretching, especially at low collision energies.

Received 1st August 2013

Accepted 10th September 2013

DOI: 10.1039/c3sc52157e

www.rsc.org/chemicalscience

Introduction

Experimental and theoretical studies on the $X + CH_4$ abstraction¹⁻⁴ and $X^- + CH_3Y$ carbon-centered bimolecular nucleophilic substitution (S_N2)⁵⁻¹⁹ reactions have extended and sometimes modified our fundamental knowledge on chemical reactivity. S_N2 reactions play an important role in organic chemistry and their Walden inversion *via* a central transition state is a well-known chemical mechanism. However, the dynamics of S_N2 reactions are sometimes more complicated due to the complexity of the global potential energy surfaces (PESs) having many stationary points such as pre- and post-reactive ion-dipole complexes and transition states between them. Furthermore, in many cases the reactions do not follow the simple pathways prescribed by the stationary points.⁷ Therefore, the atomistic details of the reaction mechanisms can only be uncovered by reaction dynamics simulations. For these simulations, knowledge of the PES is essential, because the PES governs the motion of the atoms in a chemical reaction. For the $X + CH_4$ systems, reaction dynamics computations have been performed based on high-quality analytical *ab initio* PESs;²⁻⁴

however, chemically accurate (with a relative accuracy better than 1 kcal mol^{-1}) global analytical PESs have not been developed for S_N2 reactions. Most of the previous dynamics studies on S_N2 reactions computed the electronic energies and gradients on-the-fly using low-level electronic structure methods, the inaccuracy of which may compromise the reliability of the reaction dynamics simulations.^{7,12-15,18} It is important to note, at the same time, that direct dynamics simulations have successfully reproduced many experimental findings for S_N2 reactions.¹²⁻¹⁶

As a first step toward analytical global PES-based dynamics of S_N2 reactions, in the present study we develop a chemically accurate full-dimensional *ab initio* PES for the $F^- + CH_3Cl \rightarrow Cl^- + CH_3F$ reaction and study the gas-phase dynamics of this paradigmatic S_N2 reaction. There are several features of the new PES which make our work stand out from previous studies of S_N2 reactions. We consider electron correlation up to the gold standard CCSD(T) method, basis set effects up to aug-cc-pVQZ and correlation effects of the core electrons, and fit about 37 000 *ab initio* energies covering a large configuration space and energy range. As a result, the PES accurately describes all the important C_{3v} ion-dipole complexes as well as the C_s hydrogen-bonded complexes and the transition states connecting them, and has chemical accuracy far away from the minimum energy path. This latter feature is especially important for high-energy collisions, where some direct dynamics simulations fail to

^aLaboratory of Molecular Structure and Dynamics, Institute of Chemistry, Eötvös University, H-1518 Budapest 112, P.O. Box 32, Hungary. E-mail: czako@chem.elte.hu

^bMTA-ELTE Research Group on Complex Chemical Systems, H-1117 Budapest, Pázmány Péter sétány 1/A, Hungary

provide realistic results when compared to experiments due to the inaccuracy of the low-level *ab initio* or density functional theory (DFT) computations. With this accurate PES at hand, we perform quasiclassical trajectory (QCT) calculations for the $F^- + CH_3Cl$ reaction, which may reveal several details about the reaction dynamics and mechanisms, thereby extending our chemical knowledge on fundamental polyatomic reactions at the deepest atomic and molecular levels. Our aim is to address several questions regarding the dynamics of the title reaction. How does the reactivity depend on the relative kinetic energy of the reactants? Do the pre- and/or post-reactive complexes play a role in the dynamics? How does the association depend on the initial orientation of the reactants? Can substitution happen if F^- initially approaches the Cl side of CH_3Cl ? What is the time scale of the reaction? Is there a unique mechanism of S_N2 reactions? The present dynamics simulations on the new chemically accurate PES provide definitive answers to these questions.

Methods

Potential energy surface

We develop a global PES for the $F^- + CH_3Cl$ S_N2 reaction by fitting 36 736 *ab initio* energy points obtained by an efficient composite method. 31 103 configurations are selected for the H_3CFCl^- complex region and 2181, 2182, 432, 432, and 406 points are used for the $F^- + CH_3Cl$, $Cl^- + CH_3F$, $HF + CH_2Cl^-$, $HCl + CH_2F^-$, and $FCl^- + CH_3$ channels, respectively. In order to describe the long-range ion–dipole interactions, the configuration space is covered up to ion–molecule separations of about 10 Å, resulting in about 7000 points for the substitution channel at C–F/Cl distances larger than 4 Å. Following recommendations of the focal-point analysis (FPA) technique,^{20,21} the composite energies are computed as $CCSD(T)/aug-cc-pVDZ + MP2/aug-cc-pVQZ - MP2/aug-cc-pVDZ + (AE-MP2/aug-cc-pCVTZ - FC-MP2/aug-cc-pCVTZ)$, where in parentheses the core correlation energy increment is given as a difference between all-electron (AE) and frozen-core (FC) energies. Test computations at 15 geometries show that this composite method without core correction provides AE-CCSD(T)/aug-cc-pCVQZ quality results within a root-mean-square (RMS) error of 201 cm^{-1} and this RMS reduces to only 123 cm^{-1} (0.35 kcal mol⁻¹) when we add the core correction. For comparison, the RMS errors of CCSD(T) with aug-cc-pVDZ, aug-cc-pVTZ, and aug-cc-pVQZ basis sets are 1205, 297, and 219 cm^{-1} , respectively, relative to AE-CCSD(T)/aug-cc-pCVQZ. We carry out a 5th-order fit using the permutationally invariant polynomial approach^{22,23} based on Morse-like variables, $\exp(-r_{ij}/a)$, where r_{ij} is the interatomic distance, and after some careful investigation the choice of $a = 3$ bohr is made. 3313 coefficients are obtained by a weighted linear least-squares fit using weights of $E_0/(E + E_0)$, where $E_0 = 11\,000$ cm^{-1} and the energy (E) is relative to the global minimum. The RMS fitting errors are 92, 132, and 312 cm^{-1} for the energy ranges 0–11 000, 11 000–22 000, and 22 000–55 000 cm^{-1} , respectively.

Benchmark *ab initio* thermochemistry

We compute the best technically feasible energetics for the stationary points of the title reaction utilizing the FPA approach.^{20,21} The structures and harmonic frequencies are determined at the AE-CCSD(T)/aug-cc-pCVQZ and FC-CCSD(T)/aug-cc-pVTZ levels of theory, respectively, and the energies are obtained by considering (a) extrapolation to the complete basis set limit using AE-CCSD(T)/aug-cc-pCVnZ [$n = Q(4)$ and 5] energies, (b) post-CCSD(T) correlation effects up to CCSDT(Q) based on AE-CCSDT/aug-cc-pCVDZ and FC-CCSDT(Q)/aug-cc-pVDZ energy computations, and (c) scalar relativistic effects at the second-order Douglas–Kroll²⁴ AE-CCSD(T)/aug-cc-pCVQZ level of theory. All the *ab initio* computations up to CCSD(T) are performed using the MOLPRO²⁵ program package. For the CCSDT and CCSDT(Q) computations the MRCC code,²⁶ interfaced to MOLPRO, is employed.

Quasiclassical trajectory calculations

QCT calculations are performed for the $F^- + CH_3Cl$ ($v = 0$) reaction using the new full-dimensional *ab initio* PES. The vibrational ground state ($v = 0$) of CH_3Cl is prepared by standard normal mode sampling and the rotational angular momentum (rotational temperature) of CH_3Cl is set to zero (0 K).²⁷ Trajectories are run at collision energies (E_{coll}) of 350, 700, 1400, 2450, 3500, and 5250 cm^{-1} . The initial orientation of CH_3Cl is randomly sampled and the distance between the centers of mass of the reactants is $(x^2 + b^2)^{1/2}$, where b is the impact parameter and x is 20 bohr (30 bohr at the lowest E_{coll}). b is scanned from 0 to the maximum b (b_{max}) with a step size of 1 bohr and b_{max} is found to vary between 27 and 7 bohr for the E_{coll} range of 350 to 5250 cm^{-1} . 5000 trajectories are computed at each b ; thus, the total number of trajectories at each E_{coll} is in the range of 40 000–140 000. The trajectories are propagated using a 0.0726 fs time step and each trajectory is stopped when the maximum of the actual inter-atomic distance is 1 bohr larger than the initial one. Basically no trajectory violates the product zero-point energy; thus, the QCT analysis considers all the trajectories. Normal mode analysis for the CH_3F product molecules is performed after an exact transformation to the Eckart frame and the mode-specific vibrational distributions are obtained by a novel Gaussian Binning (1GB) procedure^{28–30} as described in detail in ref. 30.

Results and discussion

Properties and accuracy of the potential energy surface

The stationary points chosen on the PES of the $F^- + CH_3Cl \rightarrow Cl^- + CH_3F$ reaction showing the benchmark quality *ab initio* structures and relative energies and the corresponding PES values are given in Fig. 1. The FPA analysis shows that the C_{3v} saddle point is below $F^- + CH_3Cl$ (eq.) by 4281 cm^{-1} , whereas the dissociation energy (D_e) of the pre-reactive C_{3v} complex is at 5467 cm^{-1} . In the entrance channel we also found a hydrogen-bonded complex (C_s symmetry) with a D_e of 5900 cm^{-1} ; thus, this C_s complex is slightly more stable than the C_{3v} one. The classical barrier height between these complexes is only

675/242 cm^{-1} relative to the C_s/C_{3v} minimum. The fact that the hydrogen-bonded complex has the deeper minimum is consistent with the finding for the $\text{F}^- - \text{CH}_4$ complex.³¹ As expected, CH_3Cl , due to its permanent dipole moment, binds F^- much more strongly than CH_4 (the D_e of $\text{F}^- - \text{CH}_4$ is only 2398 cm^{-1}).³¹ The title reaction is highly exothermic ($\Delta E_e = -11\,147 \text{ cm}^{-1}$) and there is a C_{3v} ion-dipole complex in the exit channel as well. This post-reactive complex is less stable than the pre-reactive ones, since the D_e of the former is only 3395 cm^{-1} . As also shown in Fig. 1, the analytical PES reproduces all of the FPA relative energies within chemical accuracy ($<350 \text{ cm}^{-1}$). It is remarkable that the exoergicity on the PES agrees with the FPA value within 35 cm^{-1} (0.1 kcal mol⁻¹). The benchmark C-F/C-Cl distances are 2.748/1.812, 2.613/1.826, 2.498/1.843, 2.025/2.112, and 1.413/3.180 Å for the $\text{F}^- - \text{HCH}_2\text{Cl}$ complex, $\text{F}^- - \text{HCH}_2\text{Cl}$ saddle point, $\text{F}^- - \text{CH}_3\text{Cl}$ complex, $[\text{F}^- - \text{CH}_3 - \text{Cl}]^-$ saddle point, and $\text{FCH}_3 - \text{Cl}^-$ complex, respectively (see Fig. 1), whereas the corresponding bond lengths in CH_3F and CH_3Cl are 1.383 and 1.779 Å. The structures of the stationary points on the PES are in good agreement with the accurate *ab initio* computed ones; the best agreement is found for the $[\text{F}^- - \text{CH}_3 - \text{Cl}]^-$ saddle point, where the deviations are only 0.001 Å.

In the entrance and exit channels one can expect that the ion-dipole interactions result in long-range attractive potential wells, which may play an important role in the dynamics, especially at low collision energies and large impact parameters. In Fig. 2, the potential energy curves along the C_3 axes of the $\text{ClCH}_3 - \text{F}^-$ and $\text{FCH}_3 - \text{Cl}^-$ complexes are shown. The minima are at around 2.5 and 3.2 Å, respectively, and at C-F⁻ and C-Cl⁻ separations of 3.5 and 4.5 Å the binding energies are still close

to half of the D_e . The asymptotic limits are reached at around a 10 Å ion-molecule separation. As Fig. 2 also shows, the PES describes this long-range behavior very well, since the direct *ab initio* composite energies and the PES values are in excellent agreement for both the entrance and exit channels.

As discussed above, the PES accurately describes the stationary points of the title reaction; however, the trajectories, especially at high collision energies, may not go close to the minima or saddle points. Therefore, it is important to test the accuracy of the PES far away from the stationary points. In Fig. 3, the errors of different *ab initio* levels and the PES relative to accurate AE-CCSD(T)/aug-cc-pCVQZ energies are shown at 15 configurations covering a large configuration space and an energy range up to about 18 000 cm^{-1} relative to the global minimum of the PES. As seen, all the PES points agree with the accurate reference data within 300 cm^{-1} and the RMS deviation is only 176 cm^{-1} . On the other hand, the components of the composite method, *i.e.*, CCSD(T)/aug-cc-pVDZ, MP2/aug-cc-pVDZ, and MP2/aug-cc-pVQZ, give substantial RMS errors of 1205, 938, and 633 cm^{-1} , respectively, and absolute errors larger than 1000 cm^{-1} are not rare. Furthermore, the PES (176 cm^{-1}) outperforms the CCSD(T)/aug-cc-pVTZ (297 cm^{-1}) and even the CCSD(T)/aug-cc-pVQZ (219 cm^{-1}) levels of theory, as the RMS errors in parentheses indicate. This test shows that the analytical PES has chemical accuracy at distorted structures sometimes far away from stationary points. This is an important advantage of the present PES, because many DFT methods, which are frequently used in direct dynamics simulations,^{12,13} are optimized to equilibrium and saddle-point properties, such as barrier heights and reaction enthalpies; thus, DFT may give

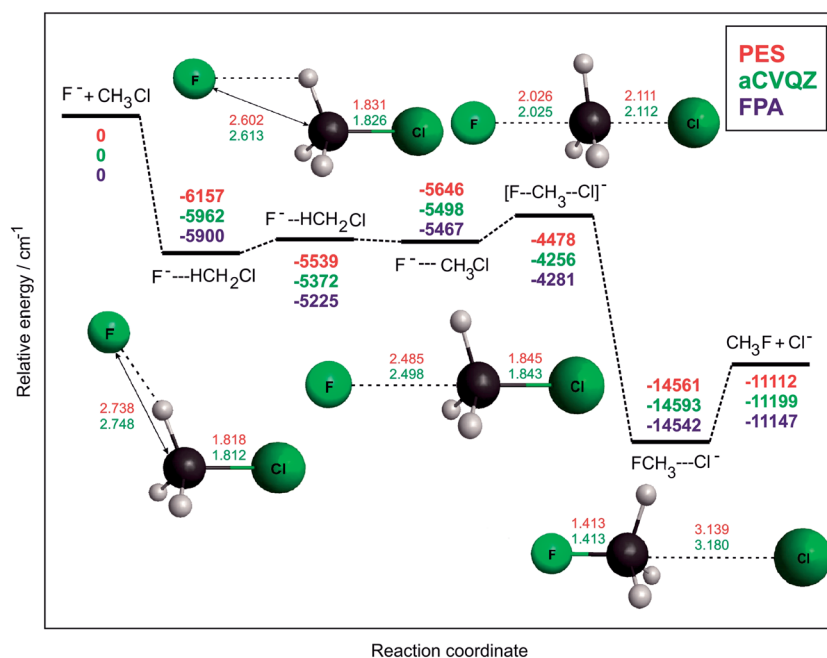


Fig. 1 Schematic representation of the potential energy surface of the $\text{F}^- + \text{CH}_3\text{Cl} \rightarrow \text{Cl}^- + \text{CH}_3\text{F}$ S_N2 reaction showing the structures and relative energies of its stationary points. The red numbers correspond to the analytical PES, the green data are obtained at the AE-CCSD(T)/aug-cc-pCVQZ level of theory providing the benchmark structures, and the blue FPA energies are of relativistic all-electron CCSDT(Q)/complete-basis-set quality. The distances are in Å and the vibrationless energies are relative to $\text{F}^- + \text{CH}_3\text{Cl}(\text{eq.})$.

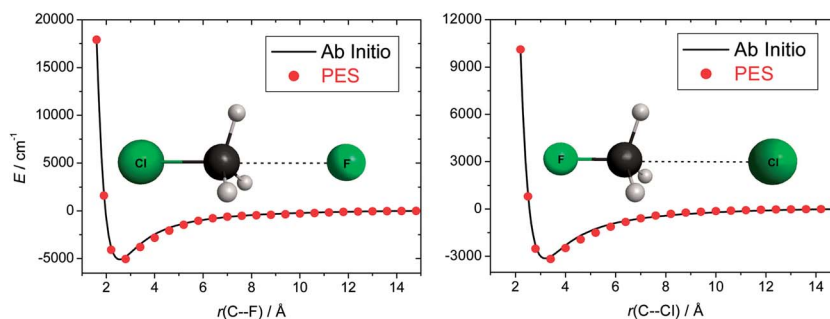


Fig. 2 Potential energy curves along the C_3 axes of $\text{ClCH}_3(\text{eq.})-\text{F}^-$ and $\text{FCH}_3(\text{eq.})-\text{Cl}^-$ showing a comparison between the direct *ab initio* composite curves and the PES values.

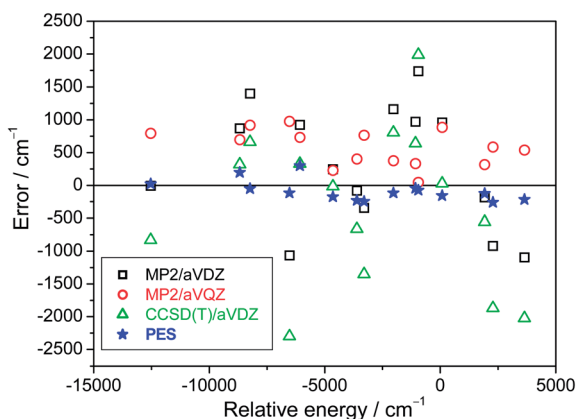


Fig. 3 Accuracy of MP2/aug-cc-pVDZ, MP2/aug-cc-pVQZ, CCSD(T)/aug-cc-pVDZ, and the analytical PES at 15 structures covering the configuration space and energy range of chemical importance. The errors are relative to the all-electron CCSD(T)/aug-cc-pVQZ energies and the energies are relative to $\text{F}^- + \text{CH}_3\text{Cl}(\text{eq.})$.

reasonable accuracy along the minimum energy path but fails at the high energy regions of the PES, thereby compromising the dynamical studies at high collision energies. Overall, our PES has an accuracy better than CCSD(T)/aug-cc-pVQZ and can be evaluated efficiently; thus, the computation of a trajectory on the PES takes only a few minutes or less of computer time. In contrast, the use of CCSD(T)/aug-cc-pVQZ energy points and gradients in direct dynamics simulations of $\text{S}_{\text{N}}2$ reactions is

simply a dream at present, since a trajectory would take many years or more to compute and one should run thousands of trajectories (we compute more than one hundred thousand in this study).

Reaction dynamics simulations

We have performed full-dimensional QCT computations for the $\text{F}^- + \text{CH}_3\text{Cl}(\nu = 0)$ reaction at different collision energies using the new PES. The opacity functions (reaction probabilities P vs. b) and the excitation function (integral cross sections (ICSs) vs. E_{coll}) are given in Fig. 4. The shapes of the opacity functions change significantly as E_{coll} increases. At collinear collisions ($b = 0$) and low values of E_{coll} , around 350–1400 cm^{-1} , the reaction probabilities are high, 60–90%, whereas $P(b = 0)$ drops to 22% at $E_{\text{coll}} = 5250 \text{ cm}^{-1}$. Furthermore, the b_{max} value shifts from 27 to 17 and 7 bohr as E_{coll} increases from 350 to 1400 and 5250 cm^{-1} . As a result, the ICS is largest at low E_{coll} and decreases rapidly with increasing E_{coll} . The reactivity at $E_{\text{coll}} = 350 \text{ cm}^{-1}$ is extremely large, the ICS is 829 bohr^2 , compared to the exothermic $\text{F} + \text{CH}_4$ reaction, which has an ICS of about 35 bohr^2 ,³² at the same E_{coll} . Furthermore, considering the slightly endothermic $\text{Cl} + \text{CH}_4$ reaction, the ICSs do not exceed 10 bohr^2 at values of E_{coll} up to 20 000 cm^{-1} .³³ The large ICSs and their negative E_{coll} dependence for the $\text{F}^- + \text{CH}_3\text{Cl}$ reaction are due to the negative barrier and the long-range attractive ion-dipole interactions allowing reactive events at large impact parameters.

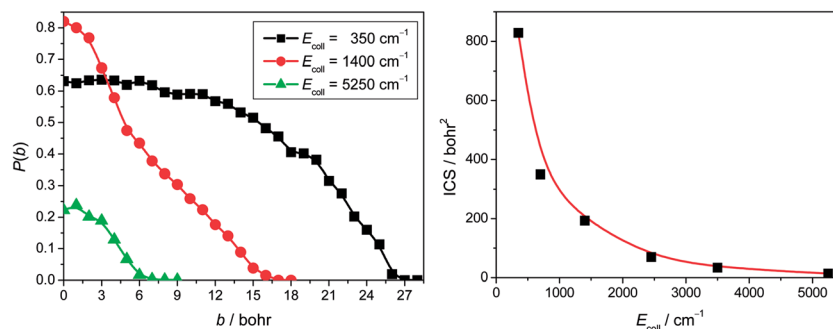


Fig. 4 Reaction probabilities as a function of impact parameter at different collision energies (left) and integral cross sections as a function of collision energy (right) for the $\text{F}^- + \text{CH}_3\text{Cl}(\nu = 0)$ reaction.

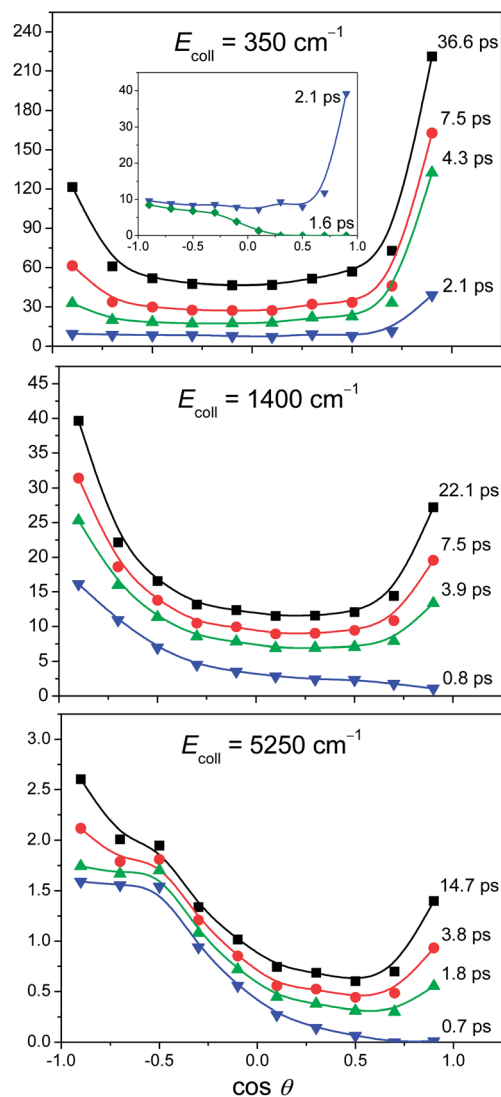


Fig. 5 Time evolution of the differential cross sections at different collision energies for the $F^- + CH_3Cl(v=0)$ reaction.

Differential cross sections (DCSs), *i.e.* cross sections as a function of $\cos \theta$, where the scattering angle θ is defined as the angle between the initial CH_3Cl and the final Cl^- velocity vectors, are given in Fig. 5. As seen, at $E_{coll} = 350 \text{ cm}^{-1}$ the angular distributions are isotropic with a small peak at backward (θ close to 180°) directions and a more substantial peak at forward (θ close to 0°) directions. At $E_{coll} = 1400 \text{ cm}^{-1}$ the dominance of the backward and forward directions over sideways scattering remains, but here the probability of backward scattering becomes preferred. At a high E_{coll} of 5250 cm^{-1} the DCS shifts toward backward directions, though a small peak at forward scattering is still seen. The trajectory simulations allow the investigation of the time evolution of the DCSs by considering only those reactive trajectories that finish until a certain time. As mentioned above, analysis of all the reactive trajectories shows a dominant peak at forward directions at $E_{coll} = 350 \text{ cm}^{-1}$. However, after a short time of 1.6 ps, forward scattering is not seen, but the DCS at the backward hemisphere

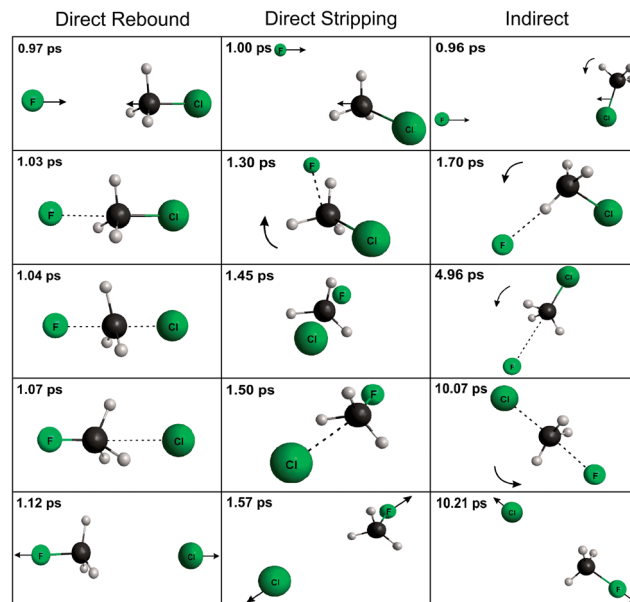


Fig. 6 Snapshots of representative trajectories illustrating the three different mechanisms of the $F^- + CH_3Cl(v=0)$ reaction at a collision energy of 350 cm^{-1} .

starts to build. After a bit longer, 2.1 ps, a clear preference of forward scattering is seen and then the forward peak increases faster than the backward one. It takes about 37 ps to get all the trajectories finished and obtain the final (experimentally observable) DCS. The shape of the DCS suggests that the title reaction occurs with different mechanisms and the time-dependent angular distributions help to identify the various pathways. The fastest trajectories go through a direct rebound mechanism, where the collisions are close to collinear (small b values) and F^- attacks the methyl side of CH_3Cl and directly substitutes Cl^- , resulting in backward scattering. This is the mechanism that can be found in every organic chemistry textbook. Another mechanism is direct stripping, which occurs at large impact parameters, typically 16–18 bohr, where F^- approaches the side of CH_3Cl and directly strips away CH_3 without changing significantly the direction of the velocity of CH_3F relative to the initial velocity of F^- , resulting in forward scattering. There is a third, indirect mechanism as well in which long-lived complexes are formed. Examination of many trajectory animations suggests that the reactants are usually trapped in the entrance channel forming hydrogen-bonded and C_{3v} ion-dipole complexes and these complexes can transform into each other frequently, as expected based on the small barrier between them. Complex formation in the exit channel is found to play a less important role in the dynamics. The long time spent in the complex region allows the overall rotation of the system, thereby randomizing the angular distributions. Representative trajectories illustrating the above-described three mechanisms are shown in Fig. 6. Note that Hase and co-workers identified similar mechanisms for the $F^- + CH_3I$ reaction employing direct dynamics simulations.¹³ As Fig. 5 shows, at the low E_{coll} of 350 cm^{-1} the appearance of backward scattering after a short time of 1.6 ps is due to the fast direct rebound

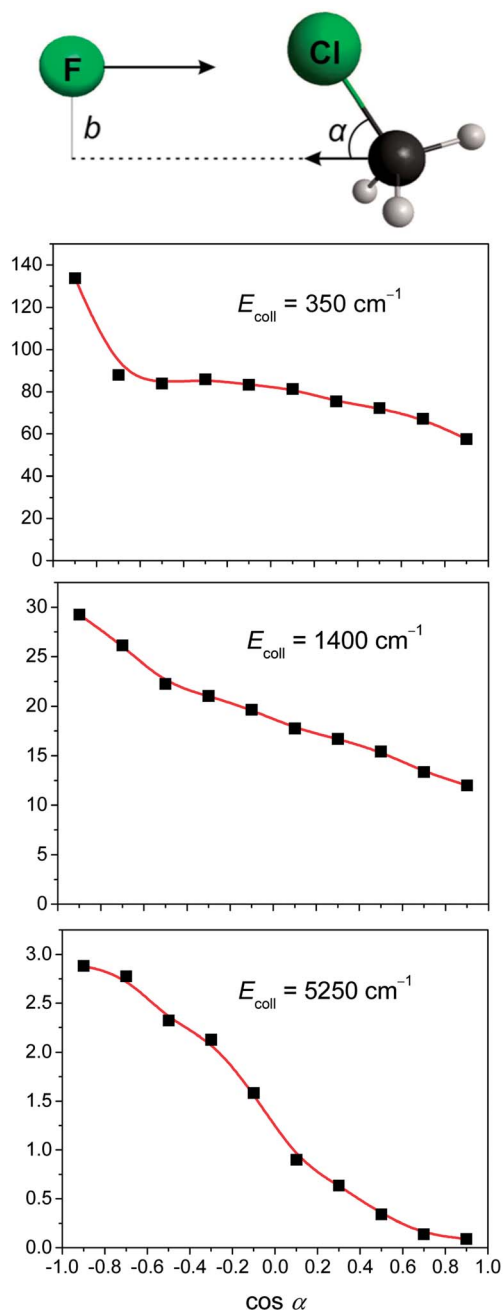


Fig. 7 Initial attack angle distributions at different collision energies for the $\text{F}^- + \text{CH}_3\text{Cl}(v = 0)$ reaction. The attack angle (α) is defined at $t = 0$ as shown in the top panel.

trajectories, then the direct stripping starts to dominate (2.1 ps) resulting in forward scattering, and at longer times the DCS builds at every direction due to the indirect mechanism. The direct stripping mechanism is responsible for the prominent forward scattering at $E_{\text{coll}} = 350 \text{ cm}^{-1}$. As E_{coll} increases, the probability of direct stripping decreases due to the decreasing b_{max} value. Note that the cross sections are obtained by a b -weighted integration of $P(b)$; thus, the stripping mechanism (large b) contributes with larger weight to the cross sections than the direct rebound trajectories (small b) do. Fig. 5 also

shows that direct rebound dominates at higher E_{coll} , especially at $E_{\text{coll}} = 5250 \text{ cm}^{-1}$, where after a short time of 0.7 ps about 60–70% of the substantial backward scattering is seen, whereas no distribution is found at forward directions. As time elapses the stripping and indirect trajectories appear resulting in forward and sideways scattering as well. Overall, the DCSs show that the title reaction is mostly direct at high E_{coll} and indirect at low E_{coll} . This finding qualitatively agrees with previous simulations on the $\text{F}^- + \text{CH}_3\text{Cl}$ reaction using a model PES,^{34,35} though our study shows substantial dominance of backward and forward directions relative to sideways scattering, which was not seen in earlier work.

We investigated the stereochemistry of the dynamics by computing the reactive cross sections as a function of the initial attack angle (α), where α is defined as the angle between the C-Cl vector and the velocity vector of CH_3Cl at $t = 0$, as shown in Fig. 7. At $E_{\text{coll}} = 350 \text{ cm}^{-1}$ the attack angle distribution is almost isotropic in the 0 – 140° range and has a significant peak close to 180° . This means that, as expected, the reactivity is larger when F^- initially approaches the face of the CH_3 group. However, this stereo-specificity is not pronounced since trajectories in which F^- approaches CH_3Cl in the non-reactive hemisphere (0 – 90°) contribute to 43% of the total cross section at $E_{\text{coll}} = 350 \text{ cm}^{-1}$. This shows that the long-range ion-dipole interactions steer the reactants into a reactive orientation even if the initial attack angle does not favor the reaction. As expected, this steering effect diminishes as E_{coll} increases; thus, 39 and 15% of the reactive events occur when the initial α is in the 0 – 90° range at E_{coll} values of 1400 and 5250 cm^{-1} , respectively. As Fig. 7 shows, at high E_{coll} initial attack angles close to 180° are clearly preferred and virtually no reaction is seen when F^- approaches the Cl atom almost collinearly. This finding is in accordance with the dominance of the direct rebound mechanism at high collision energies. On the other hand, at low E_{coll} the $\text{F}^- + \text{H}_3\text{CCl}$ trajectories are just about twice as reactive as the $\text{F}^- + \text{ClCH}_3$ collisions.

In Fig. 8 the relative translational energy (E_{trans}) distributions of the products and the correlations of E_{trans} with the velocity scattering angle distributions are shown. The E_{trans} distributions peak at low energies and as the collision energy increases a second peak emerges at high E_{trans} . At $E_{\text{coll}} = 5250 \text{ cm}^{-1}$ this second peak correlates with scattering angles in the backward hemisphere (90 – 180°) showing that the high E_{trans} corresponds to the direct rebound mechanism. The picture is similar at $E_{\text{coll}} = 1400 \text{ cm}^{-1}$; however, the correlated distribution at $E_{\text{coll}} = 350 \text{ cm}^{-1}$ shows that the higher E_{trans} correlates with forward scattering. This finding suggests that the shoulder of the E_{trans} distribution at $E_{\text{coll}} = 350 \text{ cm}^{-1}$ corresponds to the direct stripping mechanism, which results in forward scattering. The present E_{trans} distribution at $E_{\text{coll}} = 350 \text{ cm}^{-1}$ is in good agreement with that determined by Hase and co-workers³⁵ at a similar E_{coll} of 400 cm^{-1} . In their study, at a higher E_{coll} of 5650 cm^{-1} the E_{trans} distribution showed a broad peak at high energies, in agreement with the present distribution at $E_{\text{coll}} = 5250 \text{ cm}^{-1}$. However, our work shows a prominent peak at low E_{trans} , which is not seen in ref. 35.

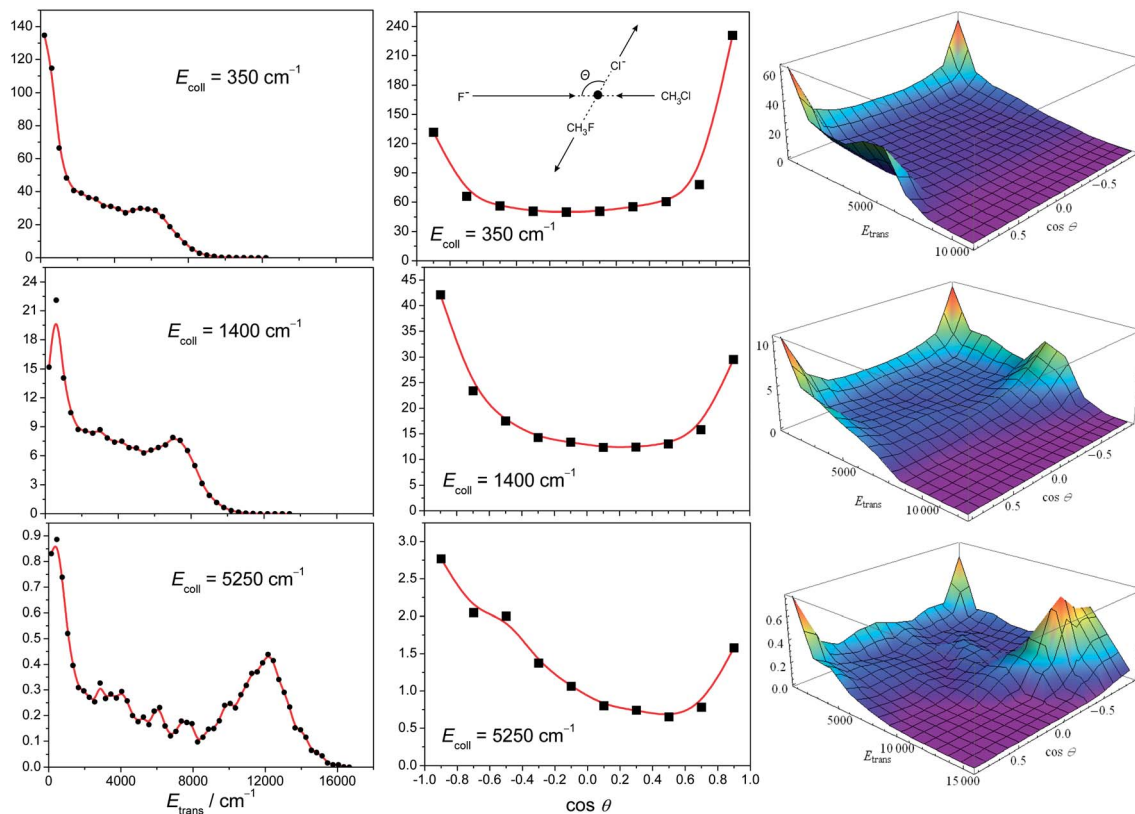


Fig. 8 Product relative translational energy distributions (left), angular distributions (middle), and their correlations (right) at different collision energies for the $F^- + CH_3Cl(v = 0)$ reaction.

The product mode-specific vibrational distributions at different collision energies are given in Fig. 9. The $F^- + CH_3Cl(v = 0)$ reaction mainly produces vibrationally highly excited CH_3F molecules; ground-state products are virtually not found. The dominant product states are the overtones of the CF stretching mode, $\nu_3(a_1)$, and their combinations with the bending modes $\nu_6(e)$ and $\nu_5(e)$ (see Fig. 9). The fact that CF stretching is excited in the product is expected, because the CF bond length is substantially stretched by 0.64 Å at the transition state relative to the corresponding equilibrium bond length in CH_3F . On the other hand, the CH bonds behave as spectators in this S_N2 reaction; consequently, the fraction of the products with excited CH stretching is negligible. At a low E_{coll} of 350 cm^{-1} the product vibrational distribution is significantly hotter than the translational energy distribution, since at low E_{coll} the indirect mechanism dominates, which minimizes the kinetic energy release and most of the available energy transfers into vibrations, in disagreement with an earlier experiment.³⁶ Our study shows that at $E_{coll} = 350\text{ cm}^{-1}$ the ν_3 mode is usually excited by 3–7 quanta and the ν_3 fundamental has negligible population. In contrast, at $E_{coll} = 5250\text{ cm}^{-1}$ most of the excess collision energy transfers into the relative translation energy of the products and the most intensive peaks in the vibrational distribution shift toward lower energies. For example, at $E_{coll} = 5250\text{ cm}^{-1}$ the population of the ν_3 fundamental becomes substantial and the dominant product states are ν_3 , $2\nu_3$, and $3\nu_3$ and their combinations with either the ν_6 or the ν_5 mode. The

overall shapes and E_{coll} dependence of the vibrational distributions agree well with the earlier results of Hase and co-workers.³⁵ Nevertheless, the previous work reported classical distributions, whereas the present study provides the quantum-state resolved vibrational distributions obtained by our novel normal-mode analysis and 1GB methods.³⁰

Summary and conclusions

Mechanisms of chemical reactions are usually investigated by locating the stationary points, *i.e.*, minima and saddle points, characterizing the corresponding potential energy surface. The minima refer to reactants, products, complexes, and/or intermediates and these minima can be connected through transition states (saddle points). The next level of sophistication is provided by minimum-energy pathways (MEPs). However, a real chemical reaction does not follow the simple MEPs between stationary points. In the case of the $X^- + CH_3Y$ S_N2 reactions the potential is a 12-dimensional surface, which governs the motion of the six atoms. The development of a chemically accurate full-dimensional PES for an S_N2 reaction, which is also accurate far away from the stationary points, has been a challenge. In this study, we have developed such a PES for the prototypical $F^- + CH_3Cl$ S_N2 reaction, and considered electron correlation up to CCSD(T), used basis sets as large as aug-cc-pVQZ, and included correlation of the core electrons. Overall, we achieved an average accuracy of 176 cm^{-1} (0.5 kcal mol⁻¹) up to about

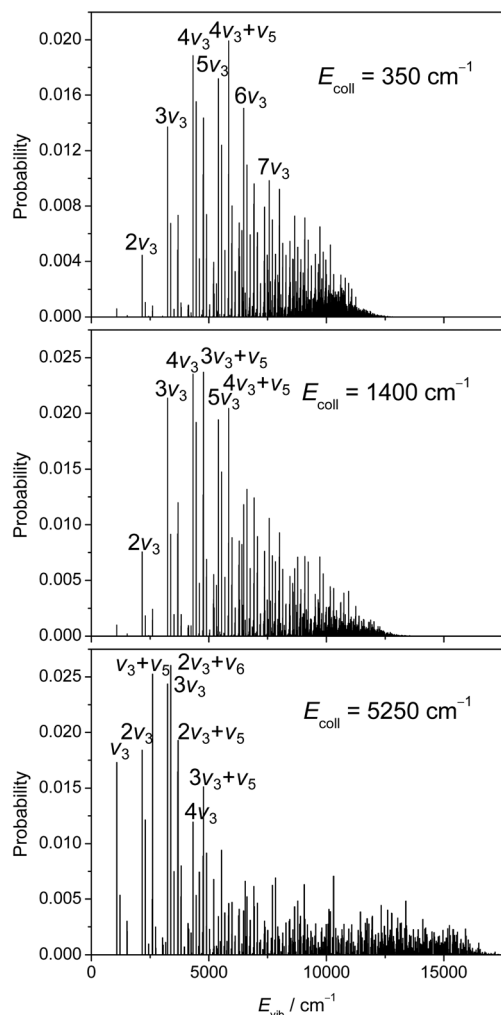


Fig. 9 Normalized CH_3F mode-specific vibrational distributions (showing all the states) at different collision energies for the $\text{F}^- + \text{CH}_3\text{Cl}(v = 0)$ reaction. The dominant product states are assigned, where $\nu_3(a_1)$ is CF stretching and $\nu_6(e)$ and $\nu_5(e)$ are bending modes with harmonic frequencies (corresponding to the PES) of 1081, 1218, and 1524 cm^{-1} , respectively. The vibrational energies are relative to the ZPE and the results are obtained by Gaussian Binning (1GB), as described in ref. 30.

18 000 cm^{-1} (50 kcal mol^{-1}) above the global minimum. This accuracy is estimated based on 15 PES points compared to all-electron CCSD(T)/aug-cc-pCVQZ reference energies.

The new PES allows efficient quasiclassical trajectory calculations to investigate the atomic-level dynamics of the $\text{F}^- + \text{CH}_3\text{Cl}$ reaction in the gas phase. Note that the dynamics may be quite different in the solution phase, but the investigation of solvent effects is out of the scope of the present study. Since the reaction is highly exothermic and has a negative barrier, the cross sections (reactivity) decrease with increasing collision energy. Based on the time evolution of the product velocity scattering angle distributions we have found that at low collision energies the indirect mechanism dominates, in which pre-reactive long-lived hydrogen-bonded and C_{3v} complexes play major roles, whereas at high collision energies the reaction mainly occurs *via* a direct rebound mechanism. Furthermore, at large impact parameters many reactive events follow a third

mechanism, direct stripping, in which F^- attacks the side of CH_3Cl and strips the CH_3 group. The trajectories also reveal that at low collision energies the long-range ion–dipole interactions steer the reactants into a reactive orientation even if F^- initially approaches the Cl side of CH_3Cl . This long-range stereochemical effect diminishes with increasing collision energy.

At low collision energies most of the available energy transfers into product vibration, populating mainly the overtones of the CF stretching mode with 3–7 quanta and their combinations with the ν_6 and ν_5 bending modes. As the collision energy increases the excess energy mainly goes to the relative translational energy of the products and the vibrational distributions shift toward lower energies, where the CF fundamental, its first and second overtones as well as their combinations with ν_6 and ν_5 bending modes are the dominant product states. Correlations of the angular and translational energy distributions reveal that the direct rebound mechanism favors translationally hot and vibrationally cold products, whereas the indirect mechanism minimizes the translational energy release and produces vibrationally excited products.

Overall, the present study shows that, unlike what is suggested in organic chemistry textbooks, the dynamics of the $\text{F}^- + \text{CH}_3\text{Cl}$ $\text{S}_{\text{N}}2$ reaction is quite complex. Sometimes it takes only 0.15 ps to get through the complex region of the PES and directly form the products, but in many cases more than 10 ps elapses until the reactants go through the pre-reactive well and the transition state region. Knowledge of an accurate full-dimensional PES is essential to investigate especially these slow indirect processes, where long-range interactions and complex formations play a major role. The present chemically accurate PES opens the door for many future dynamical investigations of the effects of isotope substitutions and reactant rotational and vibrational excitations. Quantum dynamical studies could also be performed, at least in reduced dimensions, using the new PES. Such quantum computations are desirable since QCT may allow unphysical energy transfer among the many degrees of freedom, especially for the long-lived complex-forming trajectories.³⁷ Finally, we mention that we plan to extend the present theoretical techniques to similar $\text{S}_{\text{N}}2$ reactions involving even more atoms, thereby getting deeper insight into the mechanism of these fundamental chemical reactions.

Acknowledgements

G.C. was supported by the European Union and the State of Hungary, co-financed by the European Social Fund in the framework of TÁMOP 4.2.4.A/1-11-1-2012-0001 ‘National Excellence Program’. A.G.C. thanks the Scientific Research Fund of Hungary (OTKA, NK83583) for financial support.

References

- 1 W. Zhang, H. Kawamata and K. Liu, *Science*, 2009, **325**, 303–306.
- 2 G. Czako and J. M. Bowman, *J. Am. Chem. Soc.*, 2009, **131**, 17534–17535.
- 3 G. Czako and J. M. Bowman, *Science*, 2011, **334**, 343–346.

- 4 G. Czako and J. M. Bowman, *Proc. Natl. Acad. Sci. U. S. A.*, 2012, **109**, 7997–8001.
- 5 W.-P. Hu and D. G. Truhlar, *J. Am. Chem. Soc.*, 1995, **117**, 10726–10734.
- 6 L. A. Angel and K. M. Ervin, *J. Phys. Chem. A*, 2001, **105**, 4042–4051.
- 7 L. Sun, K. Song and W. L. Hase, *Science*, 2002, **296**, 875–878.
- 8 J. K. Laerdahl and E. Uggerud, *Int. J. Mass Spectrom.*, 2002, **214**, 277–314.
- 9 M. Mugnai, G. Cardini and V. Schettino, *J. Chem. Phys.*, 2003, **118**, 2767–2774.
- 10 J. M. Gonzales, R. S. Cox III, S. T. Brown, W. D. Allen and H. F. Schaefer III, *J. Phys. Chem. A*, 2001, **105**, 11327–11346.
- 11 J. M. Gonzales, C. Pak, R. S. Cox, W. D. Allen, H. F. Schaefer III, A. G. Császár and G. Tarczay, *Chem.–Eur. J.*, 2003, **9**, 2173–2192.
- 12 J. Zhang, J. Mikosch, S. Trippel, R. Otto, M. Weidemüller, R. Wester and W. L. Hase, *J. Phys. Chem. Lett.*, 2010, **1**, 2747–2752.
- 13 J. Mikosch, J. Zhang, S. Trippel, C. Eichhorn, R. Otto, R. Sun, W. A. de Jong, M. Weidemüller, W. L. Hase and R. Wester, *J. Am. Chem. Soc.*, 2013, **135**, 4250–4259.
- 14 J. Mikosch, S. Trippel, C. Eichhorn, R. Otto, U. Lourderaj, J. X. Zhang, W. L. Hase, M. Weidemüller and R. Wester, *Science*, 2008, **319**, 183–186.
- 15 J. Zhang, U. Lourderaj, R. Sun, J. Mikosch, R. Wester and W. L. Hase, *J. Chem. Phys.*, 2013, **138**, 114309.
- 16 J. Xie, R. Sun, M. R. Siebert, R. Otto, R. Wester and W. L. Hase, *J. Phys. Chem. A*, 2013, **117**, 7162–7178.
- 17 P. Manikandan, J. Zhang and W. L. Hase, *J. Phys. Chem. A*, 2012, **116**, 3061–3080.
- 18 H. Tachikawa and M. Igarashi, *Chem. Phys. Lett.*, 1999, **303**, 81–86.
- 19 T. Su, R. A. Morris, A. A. Viggiano and J. F. Paulson, *J. Phys. Chem.*, 1990, **94**, 8426–8430.
- 20 W. D. Allen, A. L. L. East and A. G. Császár, in *Structures and Conformations of Non-Rigid Molecules*, ed. J. Laane, M. Dakkouri, B. van der Veken and H. Oberhammer, Kluwer, Dordrecht, 1993, pp. 343–373.
- 21 A. G. Császár, W. D. Allen and H. F. Schaefer, *J. Chem. Phys.*, 1998, **108**, 9751–9764.
- 22 B. J. Braams and J. M. Bowman, *Int. Rev. Phys. Chem.*, 2009, **28**, 577–606.
- 23 J. M. Bowman, G. Czako and B. Fu, *Phys. Chem. Chem. Phys.*, 2011, **13**, 8094–8111.
- 24 M. Douglas and N. M. Kroll, *Ann. Phys.*, 1974, **82**, 89–155.
- 25 H.-J. Werner, P. J. Knowles, G. Knizia, F. R. Manby, M. Schütz and others, *MOLPRO, version 2012.1, a package of ab initio programs*, see <http://www.molpro.net>.
- 26 M. Kállay, Z. Rolik, I. Ladjánszki, L. Szegedy, B. Ladóczki, J. Csontos and B. Kornis, *MRCC, a quantum chemical program suite*, See also Z. Rolik and M. Kállay, *J. Chem. Phys.*, 2011, **135**, 104111, as well as: <http://www.mrcc.hu>.
- 27 W. L. Hase, *Encyclopedia of Computational Chemistry*, Wiley, New York, 1998, pp. 399–407.
- 28 G. Czako and J. M. Bowman, *J. Chem. Phys.*, 2009, **131**, 244302.
- 29 L. Bonnet and J. Espinosa-García, *J. Chem. Phys.*, 2010, **133**, 164108.
- 30 G. Czako, *J. Phys. Chem. A*, 2012, **116**, 7467–7473.
- 31 G. Czako, B. J. Braams and J. M. Bowman, *J. Phys. Chem. A*, 2008, **112**, 7466–7472.
- 32 G. Czako and J. M. Bowman, *Phys. Chem. Chem. Phys.*, 2011, **13**, 8306–8312.
- 33 G. Czako and J. M. Bowman, *J. Chem. Phys.*, 2012, **136**, 044307.
- 34 H. Wang and W. L. Hase, *J. Am. Chem. Soc.*, 1997, **119**, 3093–3102.
- 35 T. Su, H. Wang and W. L. Hase, *J. Phys. Chem. A*, 1998, **102**, 9819–9828.
- 36 S. L. VanOrden, R. M. Pope and S. W. Buckner, *Org. Mass Spectrom.*, 1991, **26**, 1003–1007.
- 37 H. Guo, *Int. Rev. Phys. Chem.*, 2012, **31**, 1–68.